

Properties of Convective Oxygen and Silicon Burning Shells in Supernova Progenitors

Christine Collins¹★, Bernhard Müller^{2,1}†, Alexander Heger^{2,3,4}‡

¹*Astrophysics Research Centre, School of Mathematics and Physics, Queen’s University Belfast, Belfast, BT7 1NN, United Kingdom*

²*Monash Centre for Astrophysics, School of Physics and Astronomy, Monash University, Victoria 3800, Australia*

³*School of Physics & Astronomy, University of Minnesota, Minneapolis, MN 55455, U.S.A.*

⁴*Department of Astronomy, Shanghai Jiao-Tong University, Shanghai 200240, P. R. China.*

September 27, 2018

ABSTRACT

Recent three-dimensional simulations have suggested that convective seed perturbations from shell burning can play an important role in triggering neutrino-driven supernova explosions. Since isolated simulations cannot determine whether this perturbation-aided mechanism is of general relevance across the progenitor mass range, we here investigate the pertinent properties of convective oxygen and silicon burning shells in a broad range of presupernova stellar evolution models. We find that conditions for perturbation-aided explosions are most favourable in the extended oxygen shells of progenitors between about 16 and 26 solar masses, which exhibit large-scale convective overturn with high convective Mach numbers. Although the highest convective Mach numbers of up to 0.3 are reached in the oxygen shells of low-mass progenitors, convection is typically dominated by small-scale modes in these shells, which implies a more modest role of initial perturbations in the explosion mechanism. Convective silicon burning rarely provides the high Mach numbers and large-scale perturbations required for perturbation-aided explosions. We also find that about 40% of progenitors between 16 and 26 solar masses exhibit simultaneous oxygen and neon burning in the same convection zone as a result of a shell merger shortly before collapse.

Key words: supernovae: general – stars: massive – stars: evolution – convection

1 INTRODUCTION

It has long been recognised that the explosions of massive stars as core-collapse supernovae are inherently multi-dimensional phenomena (for reviews see Janka 2012; Foglizzo et al. 2015): In the modern version of the neutrino-driven explosion mechanism, multi-dimensional (multi-D) instabilities like convection (Herant et al. 1994; Burrows et al. 1995; Janka & Müller 1996) and the standing accretion shock instability (Blondin et al. 2003; Foglizzo et al. 2007) play a crucial role in boosting the efficiency of neutrino heating sufficiently to revive the shock; and for alternative scenario such as the magnetorotational mechanism, the importance of multi-dimensional effects is even more obvious. The breaking of spherical symmetry is also crucial for understanding many features of the observable transients and the compact and gaseous remnants: After shock revival, the asymmetries in the explosion determine the kick and spin of the neutron star (Janka & Müller 1994; Burrows & Hayes 1996; Fryer 2004; Scheck et al. 2006; Wongwathanarat et al.

2010; Rantsiou et al. 2011). Further multi-dimensional instabilities come into play as the shock propagates through the outer shells of the progenitor out to the stellar envelope and give rise to mixing as already recognised in the 1970s (Falk & Arnett 1973; Chevalier 1976).

Recently, multi-dimensional effects during the final stages of *presupernova* evolution have garnered particular interest in supernova theory. It has been suggested that the asymmetries seeded by convective shell burning could play an important role in tipping the scales in favour of shock revival in neutrino-driven explosions (Couch & Ott 2013; Müller & Janka 2015) by boosting the violent non-spherical motions in the gain region behind the shock upon the infall of those shells. Müller & Janka (2015) showed that the physical mechanism behind “perturbation-aided” explosions involves the conversion of the initial convective velocity perturbation into large density and ram pressure perturbations at the shock during the infall, which distort the stalled accretion shock and foster the development of large buoyant bubbles and fast non-radial flows in the gain region. They also established qualitatively that the crucial parameters for this “perturbation-aided mechanism” are the initial convective Mach number and the angular scale of the convective eddies in the progenitor; faster convective flow and larger eddies

★ E-Mail: ccollins22@qub.ac.uk

† E-mail: bernhard.mueller@monash.edu

‡ E-mail: alexander.heger@monash.edu

are more conducive to perturbation-aided explosions. Subsequent studies have attempted to put these qualitative trends on a more quantitative footing (Müller et al. 2016b; Abdikamalov et al. 2016).

The most direct way to gauge the role of convective perturbations in the progenitor in the neutrino-driven mechanism is to initialise supernova simulations properly by simulating at least the last few turnover timescales of shell convection in multiple dimensions. After a long series of two- and three-dimensional simulations of oxygen and silicon shell burning during earlier phases (Arnett 1994; Bazan & Arnett 1994, 1998; Asida & Arnett 2000; Kuhlen et al. 2003; Meakin & Arnett 2006, 2007b,a; Arnett & Meakin 2011; Jones et al. 2017), attempts to evolve convective shells up to the onset of collapse in 3D were first made by Couch et al. (2015) for silicon burning in a $15 M_{\odot}$ star, and for oxygen burning by Müller et al. (2016b) and Müller (2016) for $18 M_{\odot}$ and $12.5 M_{\odot}$ progenitors. Follow-up simulations of the collapse and post-bounce phase of the ensuing supernova with different methodology have yielded very different results ranging from a small impact on the neutrino heating conditions (Couch et al. 2015) to a large qualitative difference in Müller et al. (2017), where the perturbations prove crucial for triggering shock revival.

Such a diversity of effect sizes is not unexpected since the shell configuration and shell burning rates vary significantly among supernova progenitors. This implies that a few isolated multi-D simulations are not sufficient for determining whether convective seed perturbations generically play a major role in the supernova explosion mechanism. In addition to more extensive studies of the perturbation-aided mechanism in 3D, a more systematic investigation of the relevant parameters of shell convection across a large number of progenitors is needed, both to extrapolate the findings of the limited set of 3D studies and to help better target the 3D simulations towards interesting stellar models.

In this paper, we undertake such a study for the first time. Based on the realisation that one-dimensional stellar evolution models can be used to estimate both the violence of convection and the geometry of convective eddies even during the very dynamical phase right before the onset of collapse (Müller et al. 2016b), we investigate the systematics of the convective Mach number and the geometry of the innermost active burning shells for a set of 2,353 one-dimensional stellar evolution models (Müller et al. 2016a).

With this survey of progenitor models, we can shed light on the following questions concerning the perturbation-aided mechanism: Are pre-collapse perturbations generically strong enough to efficiently aid neutrino-driven shock revival? What mass ranges are particularly promising for perturbation-aided explosion? Are perturbations in the oxygen or silicon shell more promising for achieving shock revival? Are there unexplored scenarios that need to be simulated in 3D because some assumptions of the mixing-length approach in 1D stellar evolution models break down? Naturally, we cannot answer these questions in a definitive manner by merely considering spherically symmetric stellar evolution models; detailed 3D models of the last episodes of shell burning and the subsequent supernova explosion remain indispensable. One of the primary purposes of the present study is to provide guidance for such simulations by allowing a more targeted selection of stellar progenitor models according to the properties of the innermost convective shells.

Our paper is structured as follows: In Section 2, we briefly describe the stellar evolution models used in this study and review how convective velocities and eddy scales can be estimated from 1D models. In Section 3, we investigate systematic trends in convective Mach number and eddy scale in different shells and dis-

cuss how these are related to variations of stellar structure. We then present tentative estimates for the impact of convective perturbations on “explodability” across the stellar mass range. We conclude in Section 6 by discussing the implications of our results for future studies of the perturbation-aided explosion mechanism.

2 INPUT MODELS AND THEORETICAL BACKGROUND

2.1 Stellar Evolution Models

We consider a set of 2,353 solar-metallicity non-rotating progenitor models with zero-age main sequence (ZAMS) masses between $9.45 M_{\odot}$ and $35 M_{\odot}$ that have been computed with the stellar evolution code KEPLER (Weaver et al. 1978; Heger & Woosley 2010). This is an extension of the set of progenitors presented in Müller et al. (2016a). In these models, at $35 M_{\odot}$, the Si core mass becomes comparable to the maximum current lower limit for the maximum baryonic neutron star mass (Demorest et al. 2010; Antoniadis et al. 2016), and perturbation-aided explosions by the neutrino-driven mechanism therefore become unlikely. For this reason we do not present more massive progenitors. For high masses, however, mass loss may become important and reduce the core mass, which may affect the final outcome. We assume that the core structure of the star is not much affected by mass loss as long as some hydrogen envelope is left. Mass loss in massive stars remains somewhat uncertain, and is not the topic of this study.

The models were calculated using the standard treatment of mixing in KEPLER, i.e., convective mixing according to mixing-length theory in Ledoux-unstable regions, semiconvection according to Weaver et al. (1978), and thermohaline mixing following Heger et al. (2005). These models differ from the compilation by Sukhbold & Woosley (2014); Sukhbold et al. (2016) by updated neutrino physics that shift some of the features of late at evolution in the $15 M_{\odot} \dots 20 M_{\odot}$ region by $1 M_{\odot} \dots 2 M_{\odot}$. For numerical reasons, convective regions are bounded by one zone of overshooting with an efficiency similar to semiconvection. For the initial composition, we use the initial (in contrast to present-day) solar abundances of Asplund et al. (2009).

Following the extant studies of perturbation-aided explosions from 3D progenitors models (Couch et al. 2015; Müller 2016; Müller et al. 2017), we focus only on convection driven by Si or O burning. This is motivated by several considerations.

The O and Si shell are most likely to provide significant perturbations that can aid neutrino-driven explosions, and there is theoretical and observational evidence to suggest that shock revival occurs either during the infall of the Si or O shell. Both in multi-D supernova simulations (Suwa et al. 2016; Summa et al. 2016) and in parameterised numerical (Ugliano et al. 2012; Ertl et al. 2016) and analytic (Müller et al. 2016a), 1D models, shock revival is often associated with the infall of the Si/O shell interface, though there is also a number of cases where the explosion is initiated later during the accretion of the O shell. Delaying the explosion until the Ne or C shell reach the shock could lead to tensions with the observed distribution of neutron star masses (Schwab et al. 2010; Özel et al. 2012; Özel & Freire 2016). Moreover, the assumption of a mass cut close to the Si/O interface has been found to lead to adequate matches of the population-integrated core-collapse supernova nucleosynthesis and the solar abundance pattern (Woosley et al. 2002). We do, however, consider merged O/Ne/C shells in which both O and Ne burning are active (Section 3.3.2).

Whether shock revival occurs during the infall of the O shell or the Si shell is less clear, and our study attempts to clarify this further. Simulations as well as supernova nucleosynthesis provide circumstantial evidence that shock revival generally does not occur in the Si shell. Due to the significant neutron excess, explosive burning in the Si shell would lead, for example, to higher Ni/Fe ratios than required for chemical evolution (Arnett 1996) and than observed for most core-collapse supernovae. There are, however, exceptions among the observed core-collapse events that might be explained by ejection of material from the Si shell (Jerkstrand et al. 2015). The fact that the Si/O shell interface often acts as the trigger for shock revival in numerical models has already been mentioned, but on the theoretical side there are also examples (Müller et al. 2012) of explosions that already develop before the infall of the shell interface (even though such cases may be problematic because of modelling assumptions such as the restriction to axisymmetry). Furthermore, the point of shock revival and the “mass cut” are not strictly associated with each other in multi-D models (Harris et al. 2017; Wanajo et al. 2017), and early shock revival in the Si shell is therefore not necessarily in conflict with nucleosynthetic constraints.

Whether the pre-collapse perturbations from convective Si or O burning are dynamically more important for shock revival is also highly relevant for 3D models of the last minutes of shell burning. Due to the quasi-equilibrium nature of Si burning (Bodansky et al. 1968; Woosley et al. 1973; Hix & Thielemann 1996), rigorous 3D simulations of convective Si shells are technically more challenging. Although the basic behaviour of Si shell burning may be captured qualitatively by small networks (as in Couch et al. 2015), correctly treating the gradual shift of abundances from Si and S to the iron group and the deleptonisation requires large networks. If Si shell burning needs to be taken into account when constructing 3D supernova progenitor models, this implies a significant increase in computational cost and complexity.

For these reasons, we consider both convective Si and O shell in our progenitors in this study. There are some cases where there is more than one active convective shell driven by these burning processes (e.g., when a partially unburnt layer of O below the main O layer reignites shortly before collapse due to the contraction of the core. In these cases, we consider only the shell with the maximum convective velocity as the one that is most likely to trigger a perturbation-aided explosion.

2.2 Estimating Convective Velocities and Eddy Scales

We estimate convective velocities and Mach numbers using mixing-length theory (MLT; Biermann 1932; Böhm-Vitense 1958) and convective eddy scales based on the geometry of the convective shells assuming that the largest eddies stretch across the entire convective zone and are of similar vertical and horizontal extent. Simulations of advanced, neutrino-cooled burning stages (Kuhlen et al. 2003; Arnett et al. 2009; Müller et al. 2016b; Jones et al. 2017) suggest that the bulk properties of the 3D velocity field are reasonably well captured by these simple estimates if the dimensionless coefficients in the MLT equations are chosen appropriately.

2.2.1 Convective Velocity and Mach Number

The convective velocity v_{conv} in MLT can be expressed by

$$v_{\text{conv}} = \alpha_1 \Lambda_{\text{mix}} \omega_{\text{BV}}$$

in terms of a non-dimensional coefficient α_1 , the mixing length Λ_{mix} , and the Brunt-Väisälä frequency ω_{BV} , which, in turn, is given by

$$\omega_{\text{BV}} = \sqrt{g \left(\frac{d \ln \rho}{dr} - \frac{1}{\Gamma} \frac{d \ln P}{dr} \right)}. \quad (1)$$

Here g is the local gravitational acceleration, r is the radial coordinate, and ρ , P , and Γ are the density, pressure, and adiabatic index, respectively.

Following Müller et al. (2016b), we set the mixing length to one pressure scale height,

$$\Lambda_{\text{mix}} = \frac{P}{\rho g}, \quad (2)$$

and set $\alpha_1 = 1$, which resulted in good agreement with the convective velocities in their 3D simulation of oxygen shell burning.

A potential problem with the MLT estimate arises right before the onset of collapse when the convective turnover timescale and the contraction timescale become similar and convection can no longer adjust to the acceleration of nuclear burning during collapse. Müller et al. (2016b) found, however, that this freeze-out of convection is still captured well by 1D stellar evolution models employing time-dependent MLT so that the convective velocities from our KEPLER models remain good first-order estimates up to the onset of collapse. For a discussion of possible uncertainties in our predictions due to the use of time-dependent MLT, we refer the reader to Section 5.1

Müller & Janka (2015) showed that the relevant quantity for perturbation-aided explosion is the convective Mach number, $\text{Ma} = v_{\text{conv}}/c_s$ where c_s is the sound speed, in the progenitor rather than the convective velocity. This is because the Mach number roughly reflects the ratio of the advective crossing timescale $t_{\text{cross}} = r/v_{\text{conv}}$ and the free-fall timescale t_{ff} , which determines the density and ram-pressure perturbations at the shock after collapse. For the sake of simplicity, we therefore compute c_s assuming a constant adiabatic index of $\Gamma = 4/3$,

$$\text{Ma} = \frac{v_{\text{conv}}}{c_s} \approx \sqrt{\frac{3\rho v_{\text{conv}}^2}{4P}}, \quad (3)$$

which is a very good approximation for the convective burning shells in question. Moreover, the relation between the pre-collapse Mach number and the perturbation is not so tight as to warrant the use of the exact value of Γ ; other approximations limit our analysis and conclusions much more seriously.

2.2.2 Eddy Scale and Determination of Shell Boundaries

3D simulations of advanced shell burning stages show that the size of the largest eddies and the peak of the turbulent energy spectrum are determined by the depth of the convection zone (Arnett et al. 2009; Müller et al. 2016b), which roughly corresponds to the wavelength of the most unstable mode in the linear regime (Chandrasekhar 1961; Foglizzo et al. 2006). The dominant angular wave number, ℓ , is therefore given by

$$\ell = \frac{\pi(r_+ + r_-)}{2(r_+ - r_-)}, \quad (4)$$

where r_- and r_+ are the radius of the inner and outer boundary of a convective zone. For a given convective shell, we determine r_- and r_+ by locating the maximum of v_{conv} within that shell and then identifying the interval around that point in which v_{conv} exceeds 5% of that maximum value. This procedure was adopted to separate

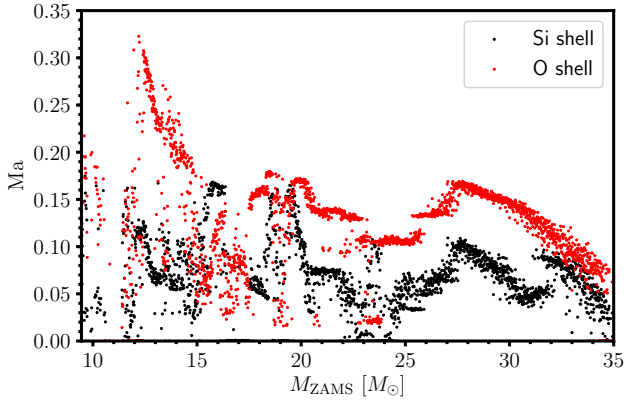


Figure 1. Maximum convective Mach number Ma in the Si (black) and O (red) shell in all progenitor models at the onset of collapse. Note that there is a trend towards higher Ma in the O shell in the less massive progenitors, and that the convective Mach number in the O shell is generally higher than in the Si shell.

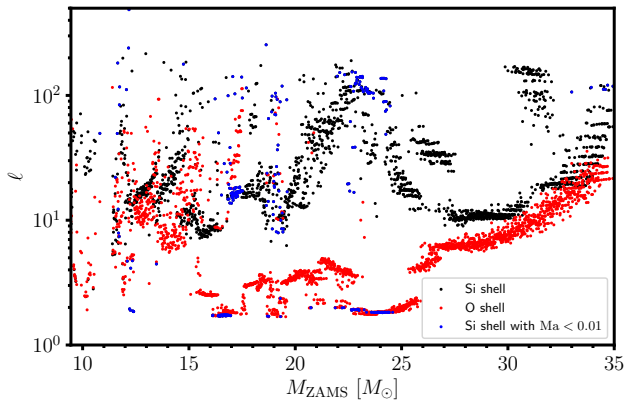


Figure 2. Predicted angular wave number ℓ of the dominant convective mode in the Si shell (black) and O shell (red) for all pre-supernova models. Si shells with very weak convection ($Ma < 0.01$) are shown in blue. Note that large-scale modes with $\ell \lesssim 5$ are largely confined to the O shells of progenitors in the mass range between $16 M_{\odot}$ and $26 M_{\odot}$.

convective zones that lie directly adjacent to each other, which is very often the case for the O and C shells.

3 RESULTS

3.1 Systematics of Convective Mach Numbers at Collapse

The convective Mach numbers in the Si shell and the O shell are shown in Figure 1 for all our progenitor models. We note that we find higher values (up to 0.3) than sometimes quoted in the literature for Si and O shell burning based on 1D stellar evolution models. This is partly due to our choice of dimensionless coefficients in Equation (1), which have been calibrated to recent 3D simulations. Moreover, quoted values of just a few 0.01 for Ma often refer to earlier stages of shell burning, and there is a considerable increase in convective velocities in the last few minutes prior to collapse as

the shells follow the contraction of the Fe core and become hotter (see, e.g., Figure 6 in Müller et al. 2016b).

Clear systematic trends in convective Mach number are evident. Convective Mach numbers in the O shell peak in the mass range of $\sim 11.5 M_{\odot} \dots 13 M_{\odot}$, where they reach values of up to 0.3, and generally decline with progenitor mass. In the vast majority of progenitors O burning drives strong convection with Mach numbers higher than 0.1. There is, however, a non-negligible fraction of progenitors that lack a strong active O shell at collapse and show only modest or weak convective activity. This is particularly true of the window between $14.5 M_{\odot}$ and $17.5 M_{\odot}$ in ZAMS mass. Above $20 M_{\odot}$, outliers with weak convection in the O shell become rare.

Convective Mach numbers in the Si shell are typically significantly smaller and lie mostly in the range $Ma = 0.05 \dots 0.1$. Ma is smaller than 0.1 in 79% of our models (assuming IMF weighting with a Salpeter IMF $\propto M^{-2.35}$ as in the rest of this paper). In 14% of the progenitors, Si shell convection is practically absent with $Ma < 0.01$.

Thus, O burning generally drives stronger convection with Mach numbers higher by a factor of 2...3 for the majority of models; the convective Mach number in the O shell exceeds that in the Si shell in 88% of our models. Exceptions include small windows around $15.5 M_{\odot}$ and $18 M_{\odot} \dots 20 M_{\odot}$ in ZAMS mass, where the convective Mach numbers in the Si shell reach up to 0.15 and equal or exceed those in the O shell.

3.2 Shell Geometry

The predicted dominant angular wave numbers of convection in the Si and O shell are plotted in Figure 2.

Small angular wave numbers, $\ell \lesssim 5$, i.e., thick convective shells, that are favourable for perturbation-aided explosions are found predominantly for O shells in progenitors between $15 M_{\odot}$ and $26 M_{\odot}$ and a small number of progenitors around $10 M_{\odot}$, and are rare outside this mass range. It is noteworthy that the O shells with high convective Mach numbers in low-mass progenitors are, for the most part, rather thin and typically have $\ell \sim 10$, although there is considerable scatter below $15 M_{\odot}$.

Active Si shells prone to low- ℓ modes in convection are rare. Only 7% of the pre-supernova models have $\ell \lesssim 5$ in the Si shell, and 84% have $\ell > 10$. Moreover, the Si shells with $\ell \lesssim 5$ invariably have weak convection with $Ma < 0.01$. Si shells with strong convection, i.e., $Ma \gtrsim 0.1$, typically have $\ell \sim 10$. In 80% of the models, we expect that Si shell burning is characterised by eddies of smaller angular scale than O shell burning at the onset of collapse.

3.3 Structural Reasons for Variations in Shell Properties

3.3.1 Effect of Core Size and Degree of Shell Depletion for O Shells

Negative entropy gradients, i.e., entropy inversions, is what drives the motion in convective regions. Usually, in the stellar interior convection is quite efficient and one would expect almost flat entropy gradients inside convection zones. Figure 3 shows the entropy profile in the O shell for a select set of models. The steep inversions toward the bottom of the O shell in the model is what drives the fast motions reported here for the collapsing O shells. This is particularly apparent for the extreme case of the $17.57 M_{\odot}$ star.

The trends mentioned in Section 3.2 cannot be reduced to a uniform underlying principle of stellar structure. Even the variations in the convective Mach number in the O shell, which exhibit

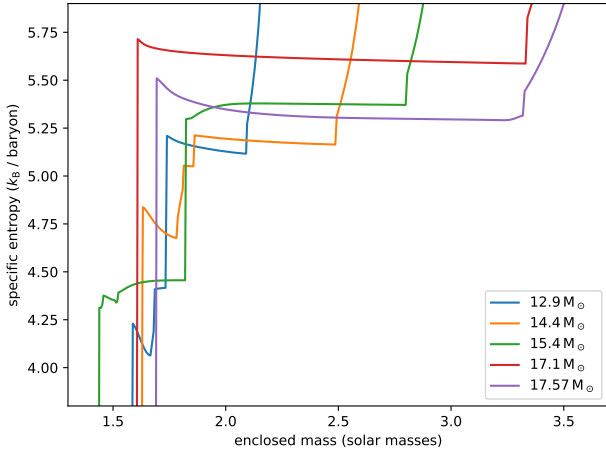


Figure 3. Specific entropy at core collapse for different initial masses. One can observe a large rise in entropy toward the bottom of the convective oxygen shell between $m = 1.5 M_{\odot}$ and $1.7 M_{\odot}$, except for the $15.4 M_{\odot}$ model, where there is only a tenuous convective shell with weak burning.

a relatively clear decreasing trend from $12 M_{\odot}$ to $25 M_{\odot}$ in ZAMS mass, are the result of a complex interplay between the varying mass and radius of the Si core, the shell entropy and density, and different degrees of shell depletion.

This is illustrated in Figure 4, which shows the (absolute value of the) gravitational potential, Gm/r ,¹ of the enclosed mass m at the base of the O shell at radius r , and the temperature T , entropy s , and oxygen mass fraction X_{O} at the base of the shell.

Except for the intervals below $\sim 12.5 M_{\odot}$ and $15.4 M_{\odot} \dots 17.5 M_{\odot}$, the convective Mach number correlates visibly with the depth of the gravitational potential at the base of the O shell and with the shell temperature, which is close to $k_{\text{B}}T = 0.3 Gmm_{\text{N}}/r$ (where k_{B} and m_{N} are the Boltzmann constant and the nucleon mass) and tends to be higher for more compact Fe-Si cores with smaller mass, higher degeneracy, and smaller radius. The key here is that the *effective* dependence of the core radius on the core mass is an inverse one and is relatively steep; thus less massive cores generate a *deeper* potential well than more massive ones. Since the O burning rate depends strongly on temperature ($\propto T^{25\dots30}$), this trend towards hotter shells around smaller cores explains the bulk of the variation in Ma in the intervals between $12.3 M_{\odot}$ and $15.4 M_{\odot}$ and $> 17.5 M_{\odot}$ in ZAMS mass.

The dependence of the O burning rate and the convective Mach number on temperature is, however, modified by variations in shell entropy and O mass fraction, in particular for ZAMS masses in the region $< 12.3 M_{\odot}$ and $15.4 M_{\odot} \dots 17.5 M_{\odot}$. In these mass ranges we encounter clusters of progenitors with high temperatures in the O shell that only exhibit weak convective activity. This is due to the fact that oxygen is close to depletion in these shells already (bottom panel of Figure 4), so that the nuclear burning rate ($\propto X_{\text{O}}^2$) is low despite high shell temperatures. This partly ex-

plains the prevalence of weak convection in the O shell in the interval $15.4 M_{\odot} \dots 17.5 M_{\odot}$, but there is also another branch of evolutionary channels in this range that has slow O shell convection for a different reason, namely low maximum shell temperatures of $\sim 3 \times 10^9$ K that occur in some merged O/Ne/C shells (see Section 3.3.2).

It is noteworthy that higher convective Mach numbers in the O shell tend to be correlated with lower shell entropies (except for the case of strongly depleted shells discussed above). The low shell entropies in models with strong convection reflect the fact that O burning occurs deeper in the gravitational potential and hence at higher temperatures also earlier on in the life of the O shell. The shell entropy can be understood as a tracer of the conditions that hold while nuclear energy generation and neutrino cooling still balance each other. In a one-zone model, the condition of balanced power (Woosley et al. 1972)

$$\dot{\epsilon}_{\text{nuc}} \sim \dot{\epsilon}_{\nu}, \quad (5)$$

for the nuclear energy generation rate $\dot{\epsilon}_{\text{nuc}}$ and the neutrino cooling rate $\dot{\epsilon}_{\nu}$, leads to

$$\rho T^{\alpha} X_{\text{O}}^2 \sim C \rho^{-1} T^{\beta} \quad (6)$$

$$\rho \propto X_{\text{O}}^{-1} (T^{(\alpha-\beta)/2}) \quad (7)$$

if we assume a power-law dependence for $\dot{\epsilon}_{\text{nuc}}$ and $\dot{\epsilon}_{\nu}$ with $\alpha \sim 27$ for O burning and $\beta \sim 9$ in the regime where neutrino cooling is dominated by the pair process. If the dominant contribution to the entropy comes from photon radiation, the entropy maintained by the shell is

$$s \propto \frac{T^3}{\rho} \propto X_{\text{O}} T^{3-(\alpha-\beta)/2} \propto X_{\text{O}} T^{-6}, \quad (8)$$

as long as the condition of balanced power holds. Since one finds $kT/m_{\text{N}} \sim 0.3 Gm/r$ in the O shell in hydrostatic equilibrium, the correlation between strong convection and low entropy in O shells is therefore expected; strong convection and low shell entropy are a reflection of the same physical reason, i.e., a smaller core size, stronger gravity, and higher temperature in the O shell.

3.3.2 Role of Shell Mergers

Very few other features in the landscape of convective Mach numbers and shell geometries admit a simple explanation. One notable exception concerns the increasing prevalence of thick convective O shells above $\gtrsim 15 M_{\odot}$. This is related to the increasing prevalence of mergers of the O, Ne, and C shells in this mass range. The tendency towards high O shell entropy in this region makes it relatively likely that the buoyancy jump between the O shell and depleted or active C/Ne shells shrinks to zero during the lifetime of the third oxygen shell, which will lead to very massive merged convection zones (often more than $1 M_{\odot}$), as illustrated in a sequence of Kippenhahn diagrams in Figure 5 for progenitors of $15.4 M_{\odot}$ (no merger), $17.1 M_{\odot}$, and $17.57 M_{\odot}$ (merger of O and C burning shells). Depending on the depletion of the C/Ne shell and the time of the merger, a rather complicated interplay of several burning processes within one deep shell can occur. Especially for late shell mergers, convective mixing is no longer sufficiently effective to homogenise the merged layers into a “pure” O burning shell. Instead, one can have a situation where the Ne produced in the C shell burns vigorously as it is mixed downwards, while O burning at the base of the shell is also active (cp. the composition of the model at collapse shown in Figure 6). Sometimes the volume-integrated nuclear energy generation rate from Ne burning becomes comparable to that

¹ At the location of the oxygen shell this is a good proxy, typically within 20% ... 30%, for the actual gravitational potential, $|\phi(r)| = Gm/r + \int_r^R Gm(r')/(r')^2 dr'$, where R and M are the radius and total mass of the stars. Moreover, Gm/r is actually correlated more tightly with shell temperature than ϕ .

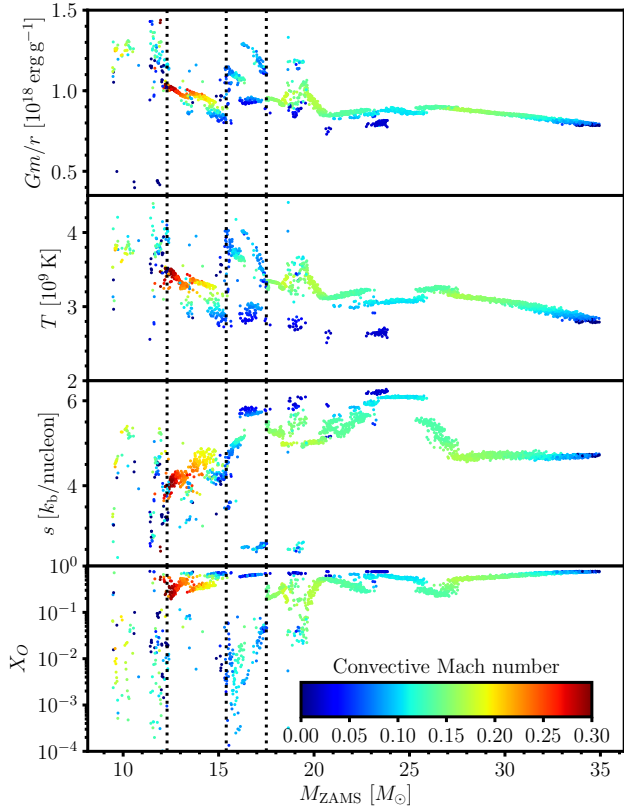


Figure 4. Key properties of convective O shells as a function of ZAMS mass M_{ZAMS} . From top to bottom: gravitational potential Gm/r of the Si core, and temperature, T , specific entropy, s , and O mass fraction X_{O} at the base of the O shell. The maximum convective Mach number in the shell is color-coded. Vertical dashed lines denote boundaries between important regimes, such as the emergence of sufficiently high X_{O} for vigorous convection above $12.3 M_{\odot}$, and the region of slow O shell convection between $15.4 M_{\odot}$, and $17.4 M_{\odot}$.

of O burning in such merged shells, especially if the temperature at the base of the shell is relatively low.² Progenitors with simultaneous O and Ne burning in the same shell at the pre-supernova stage are among the ones that exhibit the highest convective Mach numbers and the largest eddy scale. These cases are not rare; they comprise 40% of our progenitor models between $16 M_{\odot}$ and $26 M_{\odot}$.

An earlier merger (i.e. much more than a few turnover times before collapse) as in the $17.1 M_{\odot}$ model can have a very different effect: Here the merged shell has sufficient time to expand due to the energy release from the rapid burning of C and Ne from the outer shell and then maintains a relatively low temperature at its base. As a result, nuclear energy generation (mainly from the burning of O and Mg) and convection slow down, and the shell also avoids being fully mixed. Such a structural adjustment process is responsible for another part of the cases with low convective Mach numbers in the O shell above $15.4 M_{\odot}$.

² Even in these cases O burning still occurs and that Ne is fully depleted at the base of the shell, which justifies classifying them as O shells.

4 IMPACT ON THE SUPERNOVA EXPLOSION MECHANISM

Although a comprehensive and accurate quantitative theory for the interaction of perturbations in collapsing shells with the stalled accretion shock in the supernova core is still not available, numerical (Müller & Janka 2015) and analytic Abdikamalov et al. 2016; Müller et al. 2016b; Huete, Abdikamalov & Radice, in preparation) studies have established general trends: Both high Mach numbers and small angular wave numbers in the convective shell in question are required to boost the prospects for neutrino-driven explosions. Based on analytic considerations and the numerical parameter study of Müller & Janka (2015), Müller et al. (2016b) estimated that infalling perturbations reduce the critical luminosity L_{crit} (Burrows & Goshy 1993) required for a neutrino-driven runaway by

$$\frac{\Delta L_{\text{crit}}}{L_{\text{crit}}} \sim 0.47 \frac{\text{Ma}}{\ell \eta_{\text{acc}} \eta_{\text{heat}}}. \quad (9)$$

where η_{acc} is the efficiency factor for the conversion of accretion energy into electron-flavour neutrino luminosity and η_{heat} is the neutrino heating efficiency (ratio of total neutrino-heating rate and electron flavour luminosity). For typical values of $\eta_{\text{heat}} \sim 0.1$ and $\eta_{\text{acc}} \sim 2$, one obtains $\Delta L_{\text{crit}}/L_{\text{crit}} \sim 2.34 \text{Ma}/\ell$. We plot this estimated reduction of the critical luminosity due to perturbations in the Si and O shell in Figure 7. It should be emphasised that this provides only a *very rough indicator* for the prospects of perturbation-aided explosions across the stellar mass range: The theory behind Equation (9) has not yet been validated to such a degree that it could be considered as much more than a successful fit formula (Müller et al. 2017) that captures trends in extant numerical simulations of the perturbation-aided mechanism (Couch & Ott 2013; Couch et al. 2015; Müller et al. 2016b, 2017) within a factor of ~ 2 .

Fortunately, variations in $\Delta L_{\text{crit}}/L_{\text{crit}}$ are nonetheless sufficiently large to identify systematic differences between the Si and O shell and trends with progenitor mass.

The most significant finding is that O shell burning almost invariably provides more favourable conditions for perturbation-aided explosions than Si shell burning as Ma/ℓ is larger in the O shell in 91% of our progenitor models. The expected impact of perturbations from Si burning on the critical luminosity is small; effect sizes of $\sim 5\%$ are only predicted for small clusters of models around $16 M_{\odot}$ and $19 M_{\odot}$. Considering that neutrino heating conditions typically do not even get near the threshold for runaway shock expansion in sophisticated neutrino hydrodynamics simulations prior to the infall of the O shell (Summa et al. 2016; O’Connor & Couch 2015), this makes it doubtful that perturbations from the Si shell can effectively help trigger shock revival in a larger range of models. There is an important exception, however: In massive progenitors with high mass accretion rates onto the supernova shock, the SASI can develop early (Müller et al. 2012; Hanke et al. 2013; Couch & O’Connor 2014; Kuroda et al. 2016), and even a modest level of pre-shock perturbations might trigger stronger SASI activity and explosions before the infall of the O shell. Even in this scenario, the relatively large wave numbers of the perturbations in the Si shell remain an obstacle; the perturbations would not provide a strong seed for the unstable SASI modes ($\ell = 1$ or $\ell = 2$).

Perturbations from O shell are generally of a more favourable amplitude and scale for the perturbation-aided mechanism, but the expected effect size on shock revival is not uniformly high across the stellar mass range. A large reduction of the critical luminosity due to perturbations is mostly expected in the range between $\sim 16 M_{\odot}$ and $\sim 26 M_{\odot}$ with a particularly large effect size around $18 M_{\odot} \dots 19 M_{\odot}$. There are a few exceptions with high Ma and low

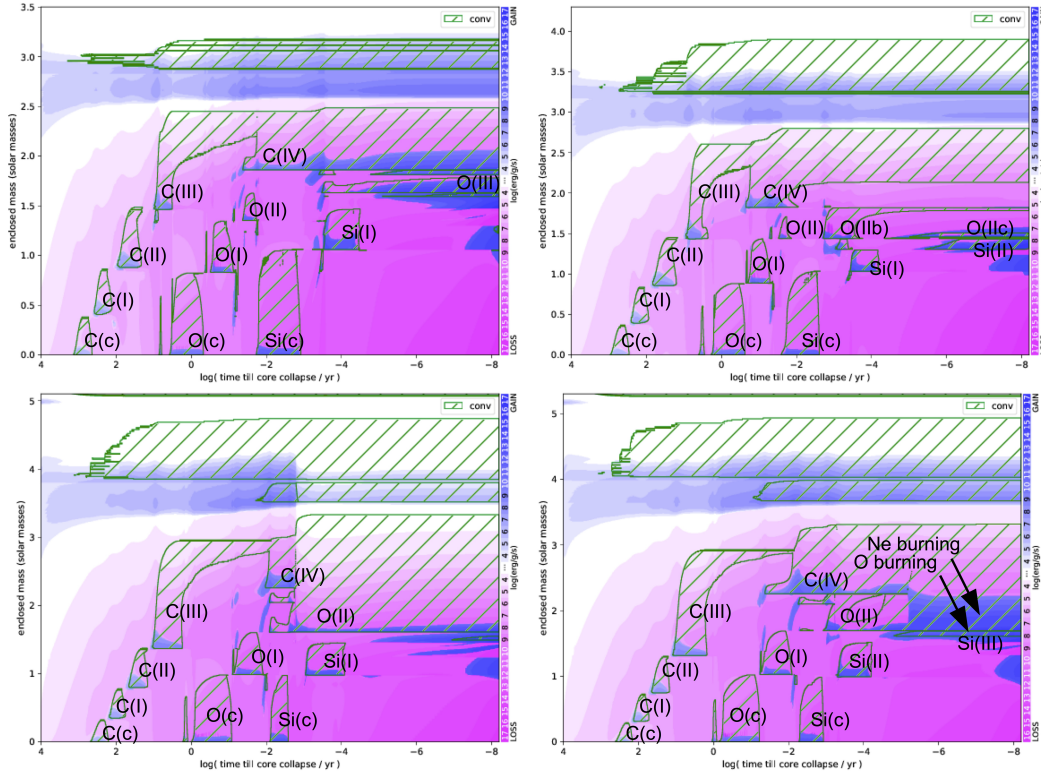


Figure 5. Kippenhahn diagrams of the last 10,000 yr of the evolution of massive stars, illustrating the transition to a different shell configuration above $16 M_{\odot}$. Convective regions (hatched) driven by Si, O, Ne, or C burning are indicated explicitly (except for very thin shells) with Roman numerals denoting the various shell burning episodes and “(c)” denoting convective core burning. Colours indicate the net energy generation/cooling rate. At low mass, the final O shell typically remains separated from the C/Ne shell regardless of whether convective burning in the C/Ne shell remains active until collapse ($14.4 M_{\odot}$ model, top left) or shuts off ($15.4 M_{\odot}$, top right). At higher mass, the O and C/Ne shell often merge ($17.1 M_{\odot}$, bottom left; $17.57 M_{\odot}$, bottom right). Typically, the outer shell in the merger is a partially burned C shell with high Ne mass fraction as depicted here. If the merger occurs early ($17.1 M_{\odot}$), there is sufficient time to mix the merged shells and largely deplete Ne or C so that the convection is only driven by the burning of O and Mg at the bottom. For late mergers (~ 10 min for $17.57 M_{\odot}$), there is insufficient time to thoroughly mix and deplete Ne or C, so that strong O and Ne burning can occur simultaneously in the same convective shell at the presupernova stage, though at different locations within that shell.

ℓ below $12 M_{\odot}$, however, with some particularly large effect sizes for progenitors around $10 M_{\odot}$. This suggests that extant studies of the perturbation-aided mechanism based on 3D progenitor models (Müller 2016; Müller et al. 2017; $18 M_{\odot}$) have already explored the most promising region in parameter space, and that the initial perturbations in the progenitor may generally play a smaller role in the explosion mechanism than the first simulations suggest. Moreover, both observations of supernova progenitors (Smartt et al. 2009; Smartt 2009, 2015) and parameterised models of neutrino-driven supernovae (O’Connor & Ott 2011; Ugliano et al. 2012; Ertl et al. 2016; Sukhbold et al. 2016; Müller et al. 2016a) indicate that the fraction of successful explosions drops strongly above $15 M_{\odot} \dots 18 M_{\odot}$. In the face of low explodability, even the strong large-scale perturbations in progenitors up to $26 M_{\odot}$ may not be sufficient to achieve shock revival in many cases.

It is interesting to note that Wongwathanarat et al. (2017) speculated about the large-scale initial perturbations as a possible explanation for asymmetries (Si- and Mg-rich “jets”) in the remnant

of Cas A that are apparently unrelated to the asymmetries of the inner Ni-rich ejecta. The fact that we find that violent large-scale convection modes in the O shell start to appear above $16 M_{\odot}$, i.e., for relatively high He core mass as suggested for the progenitor of Cas A is in line with that speculation, although simulations are needed to bear out this hypothesis.

5 UNCERTAINTIES IN SHELL PROPERTIES

As our identification of favourable and unfavourable mass ranges for perturbation-aided explosions triggered during the infall of the O or Si shell is based on 1D stellar evolution models, it is subject to uncertainties due to potential inaccuracies of MLT and the lack of a self-consistent treatment of convective boundary mixing. We argue, however, that the most serious uncertainties do not undermine our most important findings.

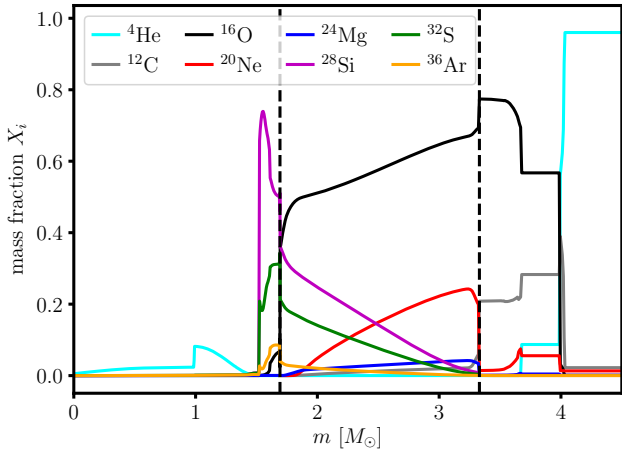


Figure 6. Mass fractions of selected elements at collapse as a function of mass coordinate in a $17.57 M_{\odot}$ model with a shell merger about 10 minutes before collapse. Dashed vertical lines denote the boundaries of the merged shell. The outer part of the shell is still Ne-rich, indicating that there is insufficient time to homogenise the shell. Ne is burned as it is mixed downwards, and any Ne is consumed before it reaches the inner shell boundary. Towards the inner shell boundary, O burning occurs, which is reflected by the steeper gradient of the O mass fraction in this region.

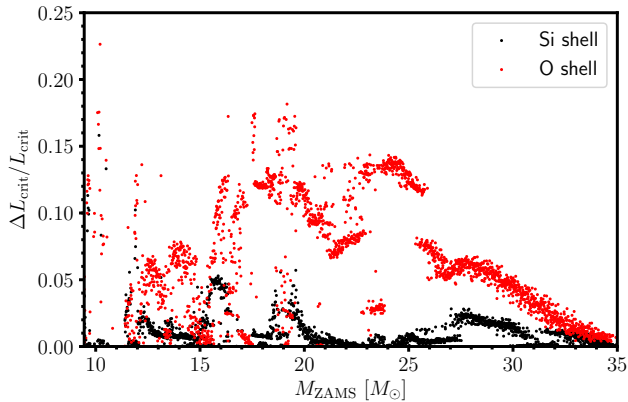


Figure 7. Estimated reduction $\Delta L_{\text{crit}}/L_{\text{crit}}$ of the critical luminosity for neutrino-driven explosions due to infalling perturbations in the Si shell (black) and O shell (red) according to Equation (9). The expected effect of perturbations on shock revival is strongest for perturbations in the O shell roughly between $16 M_{\odot}$ and $26 M_{\odot}$, and is typically small for convective perturbations in the Si shell.

5.1 Prediction of Convective Velocities

One of the problems of the MLT prediction for the convective velocity (Equation 1) lies in the use of the pressure scale height (or a multiple thereof) as the mixing length Λ_{mix} . It has been argued (Arnett et al. 2009) that the shell width is a more natural choice for Λ_{mix} considering that it sets the dominant scale of the convective eddies. Müller et al. (2016b) demonstrated, however, that the use of the pressure scale height for Λ_{mix} is justified for *thick* shells, because the condition of roughly uniform entropy generation throughout the shell for quasi-stationary convection implies that the dissipation length in the turbulent flow cannot be much

larger than the pressure scale height. For shells thinner than a pressure scale height, the standard choice for the mixing length in MLT remains questionable: Since the local value of the mixing length should be limited by the distance to the convective (Böhm & Stückli 1967; Stothers & Chin 1997), Λ_{mix} should always be bounded by the shell width. Whether MLT becomes inadequate in this regime remains to be tested by simulations, but the qualitative effect of this uncertainty on the systematics of Ma can easily be estimated. Since typical values for the pressure scale height are $r/2 \dots r/4$ in terms of shell radius r , we expect that standard MLT gives reasonable estimates for the convective Mach number for shells up to $\ell \sim 10$. Even for shells with ≥ 10 , v_{conv} should only be overestimated by a factor $\sim (\ell/10)^{1/3}$ by standard based on the dependence of v_{conv} on the cube root of the dissipation length ($v_{\text{conv}} \sim (\epsilon_{\text{nuc}} \Lambda_{\text{mix}})^{1/3}$; Arnett et al. 2009; Müller et al. 2016b; Jones et al. 2017). This implies that for the majority of O shells and the most violent Si shells, we do not expect a large error in Ma. Moreover, if the convective velocities are smaller than predicted by standard MLT, this would only accentuate our main findings, i.e., convective perturbations in the Si shell, or in the O shells of progenitors with $\sim 15 M_{\odot}$, would be even less likely to significantly boost neutrino-driven explosions.

The MLT predictions may require further study by means of 3D simulations in the case of shells with simultaneous O and Ne burning, however. That the aftermath of shell mergers may lead to interesting nucleosynthesis has already been pointed out by Ritter et al. (2017), but the flow dynamics itself also merits attention in its own right since the burning and the convective flow may depend sensitively on how Ne is mixed into the O shell. This is slightly reminiscent of a regime encountered in simulations of proton ingestion (Stancliffe et al. 2011; Herwig et al. 2011, 2014) where the burning of the entrained material can be dynamically relevant and lead to global oscillations and the establishment of a new convective boundary (Herwig et al. 2014). Although the situation is somewhat different inasmuch as the convective zones with simultaneous O and Ne burning arise from shells with a vanishing buoyancy jump, a better exploration of these shell mergers is clearly called for.

Another potential problem concerns the breakdown of a quasi-stationary balance between nuclear energy generation, buoyancy driving, and turbulent dissipation at the point when the time scale for variations in ϵ_{nuc} becomes shorter than the convective turnover time immediately before collapse (Müller et al. 2016b). Müller et al. (2016b) demonstrated, however, that time-dependent MLT still captures the “freeze-out” of convection before the onset of collapse rather well, though it can somewhat overestimate the maximum convective velocity within a shell. Again, this is unlikely to affect our central finding of stronger convection in the O shell compared to the Si shell: As the contraction of the shells outside the Fe core in the last few seconds before collapse is non-homogenous, changes in the temperatures and burning rates of Si shell are generally faster than in the O shell, and KEPLER is thus more likely to overestimate the convective velocities in Si shells where convection has already undergone freeze-out. By the same token, it is also unlikely that the ignition of unburnt Si shell can trigger strong convection during collapse. Even though the available energy from the fusion of unburnt Si during collapse is often sizable ($\sim 10^{49}$ erg), the collapse time would simply not be sufficient to allow sustained convection to develop and reach the non-linear regime; this would require convection to grow faster than on a dynamical time-scale (which is the time-scale of the collapse). Moreover, we verified that the general dependence of Ma on progenitor mass does not change substantially if we consider the average convective velocity instead

of the maximum convective velocity, which is further evidence that the systematic variations in Ma are very robust.

5.2 Uncertainties due to Convective Boundary Mixing

Compared to the uncertainties due to the use of time-dependent MLT in our stellar evolution models, it is more difficult to estimate the effect of changes in the progenitor structure due to uncertainties in convective boundary mixing. We consider it likely that convective boundary mixing does not change the overall trend towards more massive and extended Fe and Si cores and higher Fe core entropy in more massive progenitors, which is ultimately responsible for the decreasing trend in Ma .

It is, however, worth pointing out that the systematics in Ma could imply that shell growth by entrainment is stronger in low-mass progenitors and could therefore help to establish wider shells and larger convective structures in the O shells with the highest convective Mach numbers (mostly by entraining material from the C shell since the upper boundary is generally softer, see [Cristini et al. 2017](#)). In the relevant regime, the entrainment velocity v_{entr} (i.e., the velocity at which the convective boundary moves) is typically assumed to be some power law in terms of the convective velocity and the bulk Richardson number Ri_b ([Fernando 1991](#); [Strang & Fernando 2001](#); [Meakin & Arnett 2007b](#); [Cristini et al. 2016](#)),

$$v_{\text{entr}} = A v_{\text{conv}} \text{Ri}_b^{-B}, \quad (10)$$

where the coefficients A and B are still subject to debate and may be somewhat problem-dependent. In the case of a density discontinuity with a relative density jump $\Delta\rho/\rho$, Ri_b can be defined as

$$\text{Ri}_b = \frac{\Delta\rho}{\rho} \frac{gl}{v_{\text{conv}}^2} \quad (11)$$

in terms of v_{conv} , the local gravitational acceleration g , and the characteristic horizontal length scale of convection l , which we can roughly identify with Δr . With $c_s^2 \propto Gm/r$ and $l \propto r/\ell$, we find

$$\text{Ri}_b \propto \ell^{-1} \text{Ma}^{-2}. \quad (12)$$

In other words, the combination of high ℓ , v_{conv} , and Ma , which is found for O shells in progenitors below $15 M_{\odot}$ is most conducive to shell growth by entrainment. This suggests that the structure of progenitors in this mass range could be more seriously affected by convective boundary mixing, and that the O shells in these stars may be wider than estimated on the basis of our models. Considering that Ri_b varies considerably during the lifetime of shells and that the proper definition of quantities like l and $\delta\rho/\rho$ is beset with ambiguities ([Cristini et al. 2016](#)), we must refrain from investigating the behaviour of Ri_b more systematically at this stage.

6 CONCLUSIONS

We investigated the properties of convective shells in supernova progenitors at the onset of collapse with a view to the recent scenario of ‘‘perturbation-aided’’ supernova explosions ([Couch & Ott 2013](#); [Couch et al. 2015](#); [Müller & Janka 2015](#); [Müller et al. 2017](#)). Our survey of convective shells in a fine grid of 2,355 solar metallicity current single-star progenitor models computed with the stellar evolution code KEPLER ([Weaver et al. 1978](#); [Heger & Woosley 2010](#)) as first presented in [Müller et al. \(2016a\)](#) revealed that the conditions for perturbation-aided explosions are very non-uniform

across the mass range of supernova progenitors and between the O and Si burning shells.

The most favourable conditions for perturbation-aided explosions, viz. high convective Mach numbers and large-scale convective modes, are encountered in the O shells of progenitors with ZAMS masses between $\sim 16 M_{\odot}$ and $\sim 26 M_{\odot}$. An important structural reason for this is the high prevalence of mergers between the third O shell and the C or Ne shells above $16 M_{\odot}$, which leads to the formation of deep and massive O shells prior to collapse. Such mergers often occur shortly before collapse. In 40% of our progenitors between $16 M_{\odot}$ and $26 M_{\odot}$, the merger is still in progress at the onset of collapse in the sense that Ne is still not completely depleted in the shell and continues to burn while being mixed downward.

Although the highest convective Mach numbers of up to ~ 0.3 are found in the O shells of low-mass progenitors around $12 M_{\odot}$, massive shells prone to global, i.e., low- ℓ , convective modes are not very prevalent in this regime. Based on analytic arguments for the effect of perturbations on shock revival ([Müller et al. 2016b](#)), we expect convective seed asphericities to play a considerably less important role than above $16 M_{\odot}$, although the reduction of the critical luminosity for explosion due to perturbations may still be in the range of $\sim 5\% \dots 10\%$.

Favourable conditions for perturbation-aided explosions are rarely encountered in the Si shell. High convective Mach numbers ~ 0.15 and medium-scale convective modes with $\ell < 10$ are only found in a small fraction of progenitors, which mostly cluster around ZAMS masses of $16 M_{\odot}$ and $19 M_{\odot}$.

Several conclusions regarding the viability and further investigation of perturbation-aided explosions can be drawn from these findings. Although supernova simulations based on 3D initial models have only been carried out for few progenitors ($15 M_{\odot}$: [Couch et al. 2015](#), $18 M_{\odot}$: [Müller 2016](#); [Müller et al. 2017](#)), the calculations of [Müller \(2016\)](#) and [Müller et al. \(2017\)](#) have arguably probed the most promising regime for perturbation-aided explosions already, and the role of perturbations in the explosion mechanism may be more modest than appeared at first glance. Future simulations should investigate the effect of perturbations in the distinctively different regime revealed our current study, i.e., violent convection in thin O shells of low-mass progenitors and, in the case of Si shell burning, the regions around $16 M_{\odot}$ and $19 M_{\odot}$, although it needs to be borne in mind that the pattern of convective Mach numbers and eddy scales may be shifted somewhat in other stellar evolution codes. Furthermore, our findings provide justification for neglecting perturbations seeded by convective silicon burning in 3D simulations of supernova progenitors by excising the silicon core as in [Müller et al. \(2016b\)](#).

Since our study is based on spherically symmetric stellar evolution models with a time-dependent MLT treatment of convection, our findings are beset with some uncertainties that will need to be resolved by future simulations of convective burning and convective boundary mixing in the final stages of massive stars. Considering that MLT and general principles of scale selection in convection are in good agreement with detailed 3D simulations of convective shell burning ([Arnett et al. 2009](#); [Müller 2016](#)), we do not expect fundamental changes. In particular, the finding that O shell burning generally provides more favourable conditions for perturbation-aided explosions than Si burning is likely to remain robust. A more detailed investigation of 3D effects is mostly warranted in two regimes, namely for low-mass progenitors with thin oxygen shells, which should be particularly prone to strong entrainment because of the high convective Mach numbers, and shells with simultaneous O and Ne burning in massive progenitors, for which

MLT may not adequately describe the mixing of the merged shells on dynamical time scales and its interaction with the burning.

ACKNOWLEDGEMENTS

We acknowledge fruitful discussions with R. Hirschi, H.-Th. Janka, S. Sim, and S. Woosley. This work was supported by the Australian Research Council through an ARC Future Fellowships FT160100035 (BM) and Future Fellowship FT120100363 (AH) and by STFC grant ST/P000312/1 (BM). This material is based upon work supported by the National Science Foundation under Grant No. PHY-1430152 (JINA Center for the Evolution of the Elements).

References

- Abdikamalov E., Zhakyslykov A., Radice D., Berdibek S., 2016, *MNRAS*, **461**, 3864
- Antoniadis J., Tauris T. M., Ozel F., Barr E., Champion D. J., Freire P. C. C., 2016, preprint, ([arXiv:1605.01665](https://arxiv.org/abs/1605.01665))
- Arnett D., 1994, *ApJ*, **427**, 932
- Arnett D., 1996, *Supernovae and Nucleosynthesis: An Investigation of the History of Matter from the Big Bang to the Present*. Princeton: Princeton University Press
- Arnett W. D., Meakin C., 2011, *ApJ*, **733**, 78
- Arnett D., Meakin C., Young P. A., 2009, *ApJ*, **690**, 1715
- Asida S. M., Arnett D., 2000, *ApJ*, **545**, 435
- Asplund M., Grevesse N., Sauval A. J., Scott P., 2009, *ARA&A*, **47**, 481
- Bazan G., Arnett D., 1994, *ApJ*, **433**, L41
- Bazan G., Arnett D., 1998, *ApJ*, **496**, 316
- Biermann L., 1932, *Z. Astrophys.*, **5**, 117
- Blondin J. M., Mezzacappa A., DeMarino C., 2003, *ApJ*, **584**, 971
- Bodansky D., Clayton D. D., Fowler W. A., 1968, *ApJS*, **16**, 299
- Böhm K.-H., Stückl E., 1967, *Z. Astrophys.*, **66**, 487
- Böhm-Vitense E., 1958, *Z. Astrophys.*, **46**, 108
- Burrows A., Goshy J., 1993, *ApJ*, **416**, L75+
- Burrows A., Hayes J., 1996, *Physical Review Letters*, **76**, 352
- Burrows A., Hayes J., Fryxell B. A., 1995, *ApJ*, **450**, 830
- Chandrasekhar S., 1961, *Hydrodynamic and Hydromagnetic Stability*. Clarendon, Oxford
- Chevalier R. A., 1976, *ApJ*, **207**, 872
- Couch S. M., O'Connor E. P., 2014, *ApJ*, **785**, 123
- Couch S. M., Ott C. D., 2013, *ApJ*, **778**, L7
- Couch S. M., Chatzopoulos E., Arnett W. D., Timmes F. X., 2015, *ApJ*, **808**, L21
- Cristini A., Meakin C., Hirschi R., Arnett D., Georgy C., Viallet M., 2016, *Phys. Scr.*, **91**, 034006
- Cristini A., Meakin C., Hirschi R., Arnett D., Georgy C., Viallet M., Walkington I., 2017, *MNRAS*, **471**, 279
- Demorest P. B., Pennucci T., Ransom S. M., Roberts M. S. E., Hessels J. W. T., 2010, *Nature*, **467**, 1081
- Ertl T., Janka H.-T., Woosley S. E., Sukhbold T., Ugliano M., 2016, *ApJ*, **818**, 124
- Falk S. W., Arnett W. D., 1973, *ApJ*, **180**, L65
- Fernando H. J. S., 1991, *Annual Review of Fluid Mechanics*, **23**, 455
- Foglizzo T., Scheck L., Janka H.-T., 2006, *ApJ*, **652**, 1436
- Foglizzo T., Galletti P., Scheck L., Janka H.-T., 2007, *ApJ*, **654**, 1006
- Foglizzo T., et al., 2015, *Publ. Astron. Soc. Australia*, **32**, e009
- Fryer C. L., 2004, *ApJ*, **601**, L175
- Hanke F., Müller B., Wongwathanarat A., Marek A., Janka H.-T., 2013, *ApJ*, **770**, 66
- Harris J. A., Hix W. R., Chertkow M. A., Lee C.-T., Lentz E. J., Messer O. E. B., 2017, *ApJ*, **843**, 2
- Heger A., Woosley S. E., 2010, *ApJ*, **724**, 341
- Heger A., Woosley S. E., Spruit H. C., 2005, *ApJ*, **626**, 350
- Herant M., Benz W., Hix W. R., Fryer C. L., Colgate S. A., 1994, *ApJ*, **435**, 339
- Herwig F., Pignatari M., Woodward P. R., Porter D. H., Rockefeller G., Fryer C. L., Bennett M., Hirschi R., 2011, *ApJ*, **727**, 89
- Herwig F., Woodward P. R., Lin P.-H., Knox M., Fryer C., 2014, *ApJ*, **792**, L3
- Hix W. R., Thielemann F.-K., 1996, *ApJ*, **460**, 869
- Janka H.-T., 2012, *Annual Review of Nuclear and Particle Science*, **62**, 407
- Janka H.-T., Müller E., 1994, *A&A*, **290**, 496
- Janka H.-T., Müller E., 1996, *A&A*, **306**, 167
- Jerkstrand A., et al., 2015, *ApJ*, **807**, 110
- Jones S., Andrassy R., Sandalski S., Davis A., Woodward P., Herwig F., 2017, *MNRAS*, **465**, 2991
- Kuhlen M., Woosley W. E., Glatzmaier G. A., 2003, in Turcotte S., Keller S. C., Cavallo R. M., eds, *Astronomical Society of the Pacific Conference Series Vol. 293, 3D Stellar Evolution*. p. 147
- Kuroda T., Kotake K., Takiwaki T., 2016, *ApJ*, **829**, L14
- Meakin C. A., Arnett D., 2006, *ApJ*, **637**, L53
- Meakin C. A., Arnett D., 2007a, *ApJ*, **665**, 690
- Meakin C. A., Arnett D., 2007b, *ApJ*, **667**, 448
- Müller B., 2016, *Publ. Astron. Soc. Australia*, **33**, e048
- Müller B., Janka H.-T., 2015, *MNRAS*, **448**, 2141
- Müller B., Janka H.-T., Heger A., 2012, *ApJ*, **761**, 72
- Müller B., Heger A., Liptai D., Cameron J. B., 2016a, *MNRAS*, **460**, 742
- Müller B., Viallet M., Heger A., Janka H.-T., 2016b, *ApJ*, **833**, 124
- Müller B., Melson T., Heger A., Janka H.-T., 2017, preprint, ([arXiv:1705.00620](https://arxiv.org/abs/1705.00620))
- O'Connor E., Couch S., 2015, preprint, ([arXiv:1511.07443](https://arxiv.org/abs/1511.07443))
- O'Connor E., Ott C. D., 2011, *ApJ*, **730**, 70
- Özel F., Freire P., 2016, *ARA&A*, **54**, 401
- Özel F., Psaltis D., Narayan R., Santos Villarreal A., 2012, *ApJ*, **757**, 55
- Rantsiou E., Burrows A., Nordhaus J., Almgren A., 2011, *ApJ*, **732**, 57
- Ritter C., Andrassy R., Côté B., Herwig F., Woodward P. R., Pignatari M., Jones S., 2017, preprint, ([arXiv:1704.05985](https://arxiv.org/abs/1704.05985))
- Scheck L., Kifonidis K., Janka H.-T., Müller E., 2006, *A&A*, **457**, 963
- Schwab J., Podsiadlowski P., Rappaport S., 2010, *ApJ*, **719**, 722
- Smartt S. J., 2009, *ARA&A*, **47**, 63
- Smartt S. J., 2015, *Publ. Astron. Soc. Australia*, **32**, 16
- Smartt S. J., Eldridge J. J., Crockett R. M., Maund J. R., 2009, *MNRAS*, **395**, 1409
- Stancliffe R. J., Dearborn D. S. P., Lattanzio J. C., Heap S. A., Campbell S. W., 2011, *ApJ*, **742**, 121
- Stothers R. B., Chin C.-w., 1997, *ApJ*, **478**, L103
- Strang E. J., Fernando H. J. S., 2001, *Journal of Fluid Mechanics*, **428**, 349
- Sukhbold T., Woosley S. E., 2014, *ApJ*, **783**, 10
- Sukhbold T., Ertl T., Woosley S. E., Brown J. M., Janka H.-T., 2016, *ApJ*, **821**, 38
- Summa A., Hanke F., Janka H.-T., Melson T., Marek A., Müller B., 2016, *ApJ*, **825**, 6
- Suwa Y., Yamada S., Takiwaki T., Kotake K., 2016, *ApJ*, **816**, 43
- Ugliano M., Janka H.-T., Marek A., Arcones A., 2012, *ApJ*, **757**, 69
- Wanajo S., Müller B., Janka H.-T., Heger A., 2017, preprint, ([arXiv:1701.06786](https://arxiv.org/abs/1701.06786))
- Weaver T. A., Zimmerman G. B., Woosley S. E., 1978, *ApJ*, **225**, 1021
- Wongwathanarat A., Janka H., Müller E., 2010, *ApJ*, **725**, L106
- Wongwathanarat A., Janka H.-T., Müller E., Pllumbi E., Wanajo S., 2017, *ApJ*, **842**, 13
- Woosley S. E., Arnett W. D., Clayton D. D., 1972, *ApJ*, **175**, 731
- Woosley S. E., Arnett W. D., Clayton D. D., 1973, *ApJS*, **26**, 231
- Woosley S. E., Heger A., Weaver T. A., 2002, *Rev. Mod. Phys.*, **74**, 1015